

Photon Emission from Hollow Ions Near Surfaces

Stephan Fritzsche ^{1,2,3} ¹ Helmholtz-Institut Jena, Fröbelstieg 3, D-07743 Jena, Germany; s.fritzsche@gsi.de² GSI Helmholtzzentrum für Schwerionenforschung, D-64291 Darmstadt, Germany³ Theoretisch-Physikalisches Institut, Friedrich-Schiller-Universität Jena, D-07743 Jena, Germany

Abstract: Ions with multiple inner-shell vacancies frequently arise due to their interaction with different targets, such as (intense) light pulses, atoms, clusters or bulk material. They are formed, in addition, if highly charged ions approach surfaces and capture electrons at rather large distances. To explore the interaction of such hollow ions and their subsequent relaxation, photon spectra in different frequency regions have been measured and compared to calculations. To support these and related measurements, we here show within the framework of the Jena Atomic Calculator (JAC) how (additional) electrons in outer shells modify photon emission and lead to characteristic shifts in the observed spectra. Further, for highly charged Ar ions in KL^m ($m = 1 \dots 8$) configurations, we analyze the mean relaxation time for their stabilization into the different ground configurations. These examples demonstrate how a powerful and flexible toolbox such as JAC will be useful (and necessary) in order to model the photon and electron emission of ions as they occur not only near surfaces but also in astro-, atomic and plasma physics.

Keywords: atom; atomic cascade; electron capture; hollow ion; ion-surface interaction; Jena Atomic Calculator; line shape; photon emission; relativistic

1. Introduction

Hollow atoms were initially introduced as a term in surface physics by Briand et al. [1] in the late 1980s in order to explain the soft X-ray emission observed from the impact of 340 keV Ar^{17+} ions on a gas-covered silver surface. Since then, the formation and decay of such hollow atoms have been studied in great detail and have been shown to occur both above and below the surface [2]. Because of their large coulomb energy, these ions capture electrons from the surface and quickly stabilize by electron and photon emission, while they remain nearly neutral during their relaxation by exchanging more and more electrons. To understand the stabilization dynamics of such hollow ions, both the electron and photon spectra have been observed and were analyzed on the basis of calculated energies and Auger rates [3,4]. Whereas the charge transfer of weakly bound electrons from a metal surface already sets in at rather large distances, the guiding of multiply charged particles through insulating capillaries has shown that the ions never contact the inner surface, but built-up charged patches at different places along the capillary wall [5,6]. Further interest in the formation and decay of hollow ions and atoms arises from astro- [7,8] and plasma physics [9] as well as from precision measurements [10], where they may resolve a controversy about quantum electrodynamic (QED) calculations recently brought up by Chantler and coworkers [11].

While the capture of electrons by slow ions can be understood by classical arguments, the relaxation of the multiply excited states remains difficult to model and usually results in complex spectra. In particular, Wilhelm et al. [12] determined experimentally the time constants for the neutralization and de-excitation of highly charged ions to about 1–3 fs and, hence, concluded that the formation and subsequent decay mainly proceed via inter-coulombic decay [13,14]. Indeed, these experiments indicate that the current model of the formation and de-excitation of hollow ions has to be refined further as the atomic cascades alone are too slow [4,15]. While analysis of electron spectra are often hampered by the



Citation: Fritzsche, S. Photon Emission from Hollow Ions Near Surfaces. *Atoms* **2022**, *10*, 37. <https://doi.org/10.3390/atoms10020037>

Academic Editor: Károly Tőkési

Received: 12 March 2022

Accepted: 7 April 2022

Published: 10 April 2022

Publisher's Note: MDPI stays neutral with regard to jurisdictional claims in published maps and institutional affiliations.



Copyright: © 2022 by the authors. Licensee MDPI, Basel, Switzerland. This article is an open access article distributed under the terms and conditions of the Creative Commons Attribution (CC BY) license (<https://creativecommons.org/licenses/by/4.0/>).

given setup of the experiments, the observed photon spectra may help to investigate this dynamic when compared to proper calculations. In particular the photon spectra from the filling of the K- and L-shell vacancies in an early stage of the stabilization may provide further insight into the process.

In this work, we analyze how the excitation or placement of additional electrons in different valence shells affects the subsequent photon emission from multiply charge ions. This analysis is made independent of the particular capture process of the electrons and by assuming an always stable ionic core that is surrounded by one or several electrons in outer shells. As a special case, of course, this also includes an empty core with no K-shell electrons at all. All photon spectra below are simulated within the framework of the Jena Atomic Calculator (JAC) [16,17], which supports the (relativistic) computation of atomic structures and processes. This toolbox has been enlarged in this work in order to model the photon emission spectra from such hollow ions with (any number of) additional electrons in outer shells. The separation of the initial capture from the subsequent atomic decay processes enables us to explore hollow ions under quite different circumstances and to extract the associated electron and photon spectra. In the next section, we first summarize how selected spectra can be simulated and are modified by the stepwise decay of these hollow ions. We also briefly introduce the JAC toolbox and its underlying design, which provides a descriptive language for modeling atomic and hollow-ion cascades of quite different complexity. Detailed computations are carried out and discussed in Section 3 for the $K\alpha$ photon emission of initially Ar^{17+} ions but with additional electrons in the L and M shells. For selected KL^m ($m = 1 \dots 8$) configurations of Ar^{q+} ($q = 9 \dots 16$), as an example, we also explore the mean relaxation time for their stabilization into the ground configuration and shall discuss further computational tasks for simulating photon emission from hollow ions. Finally, a short summary and conclusions are given in Section 4.

2. Modeling Photon Emission from Hollow Ions

2.1. Photon Absorption and Emission

For weak photon fields, the electron-photon interaction is quite well understood, both in non-relativistic and relativistic theory [18]. Its quantum description is typically built upon the generation of approximate atomic state functions (ASF) as well as the computation of photon absorption and emission amplitudes for all the levels involved in some process or cascade [19,20]. Not much needs to be said about the basic theory, which can be found in various texts; cf. Ref. [21]. Here, we shall apply a multiconfiguration Dirac–Hartree–Fock expansion of all ASF in terms of symmetry-adopted configuration state functions (CSF) and, especially, their implementation within the JAC toolbox [16,22].

To make use of these amplitudes for simulating (and analyzing) the photon emission spectra from atoms and ions in quite different initial configurations, an explicit and frequently applied notation of all (reduced) emission and absorption multipole matrix elements in the JAC program is

$$\langle \alpha_f \mathbb{J}_f \parallel \circlearrowleft^{(\mathbb{M}, \text{emission})} \parallel \alpha_i \mathbb{J}_i \rangle = \left\langle \alpha_i \mathbb{J}_i \parallel \sum_{k=1}^N \alpha_k a_{k,L}^p \parallel \alpha_f \mathbb{J}_f \right\rangle^* \equiv \langle \alpha_i \mathbb{J}_i \parallel \circlearrowleft^{(\mathbb{M}, \text{absorption})} \parallel \alpha_f \mathbb{J}_f \rangle^*, \quad (1)$$

where we aim for all (single-step) processes to always retain the correct quantum-mechanical order of the initial ($\alpha_i \mathbb{J}_i$) and final ($\alpha_f \mathbb{J}_f$) levels in going from right-to-left in the associated transition amplitudes. Here, $\mathbb{J} \equiv J^P$ is a short-hand notation of both the total angular momentum J and the parity P of the many-electron levels, while α refers to all further quantum numbers that are needed in order to determine the atomic states uniquely. In this notation, furthermore, $\mathbb{M} \equiv (L, p) = \{E1, M1, E2, \dots\}$ simply denotes a selected multipole component of the radiation field and, thus, comprises information about its multipolarity L as well as the type of the radiative transition, i.e., $p = 0$ for magnetic and $p = 1$ for electric multipole transitions. Indeed, the transition amplitudes in Equation (1) as well as a few others (cf. Figure 1) are the *building blocks* of the JAC toolbox and enable

one to model complex decay cascades as they occur for hollow ions and at many places elsewhere [17].

Often and in good approximation for all photon emission and autoionization processes, the atomic levels are described within the atomic shell model, in which the occupation of (sub-) shells is simply given by leading electron configurations, such as $1s2p(3s^2 + 3s3p + 3s3d + 3p^2 + 3p3d + 3d^2)$ in order to denote the $KL_{23}M^2$ configurations, following their capture into the L and M shells. The use of these (electron) configurations has been found crucial in order to make atomic cascades *computable* and to extract beneficial information about all the associated processes and spectra [18,23].

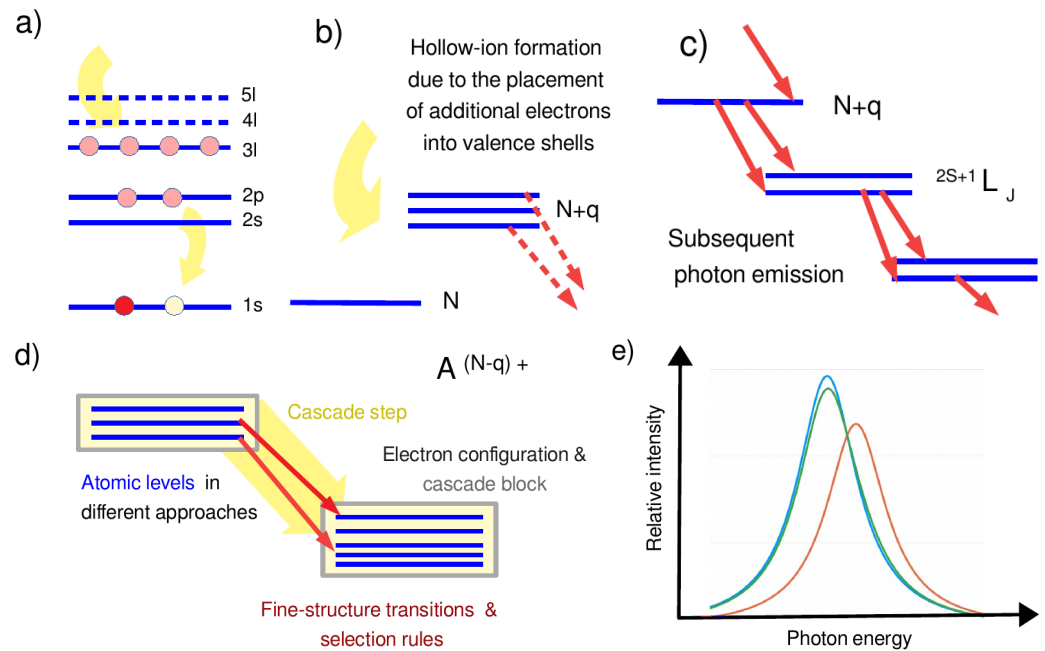


Figure 1. Photon emission of multiply excited ions following the placement of additional electrons into outer nl shells. (a) Single-particle view upon capture of one or several electrons into the L_{23} and M shells of initially hydrogen-like ions. (b) Associated many-particle view upon the formation of excited ions with q additional electrons in different nl shells, and where (c) each electron configuration with a well-defined population of the shells gives rise to a multiplet of terms and fine-structure levels $2S+1L_J$ (blue lines) as well as to photon transitions (red arrows) that connect these levels. (d) Modeling of photoemission cascades from such hollow ions in terms of electron configurations, fine-structure multiplets (cascade blocks) and transition amplitudes based on the well-known selection rules, and which altogether determine the observed photon emission. (e) Schematic shift and broadening of, for example, the $K\alpha_{12}$ lineshape owing to additional electrons in nl valence shells. See text for further discussion.

2.2. Photon Cascades and Spectra Following Multiple Electron Capture

Photon spectra from multiply charged ions are ubiquitous in nature and arise at quite different frequency regions because the emission of photons is an important de-excitation mechanism in the stabilization of atoms and ions towards their ground level [24]. Such photon spectra also occur, for instance, after photoexcitation and particle impact (by electrons, positrons, protons, etc.), or the capture of electrons. For the placement of electrons into shells with medium and high principal quantum n , especially, their stepwise decay towards the ground level typically results in an “emission spectrum” that is characteristic of the initial distribution of the electrons among the occupied subshells. Moreover, since the Einstein coefficients $A_{ik} \propto \omega_{ik}^3 \propto n^{-3}$ roughly scale for a fixed ionic core inversely with the third power of n , electrons in shells with a large principal quantum number may survive the radiative decay (cascade) of deeper bound electrons by just staying as spectators

in some outer shell, and by giving rise to small line shifts that are not always easy to detect experimentally.

For the multiple capture of electrons into medium and high- n shells, indeed, a reasonably large fraction of electrons either remain in their shells or decay just stepwise towards the ground configuration. For the double electron capture into $n = 4 \dots 7$ shells of hydrogen-like argon ion, for example, it was found that one of the electrons cascades down, while the other remains rather much in its initial shell [25]. In practice, however, very little is known so far how additional electrons affect the detailed photon emission after core-shell excitations or how long it takes for such ions to relax down to their ground configuration. Moreover, (slightly) shifted line positions and shapes are expected, if either a core-excitation occurs for different initial populations of the valence shells or at different times after that the electron capture has occurred.

To shine further light on the photon emission of ions with one or several electrons in outer shells, we here develop and implement a cascade model for (so-called) hollow ions that is based on a detailed treatment of the fine-structure of all electron configurations as they are populated during the subsequent decay of the ions. Such a cascade usually includes ions of the same element but in different charge states, which are connected to each other by different atomic processes, such as electron capture, autoionization or photon emission, to mention just a few. Figure 1 shows the photon emission of multiply excited ions following the placement of one or several electrons into outer shells. Apart from the single-particle view for placing electrons into the L_{23} and M shells of, for instance, initially hydrogen-like Ar^{17+} ions (a), a many-particle view exhibits the formation and distribution of the fine-structure levels associated with each configuration (b) as well as the photon emission between these levels (c). Since the number of fine-structure levels increases very rapidly with the number of open subshells, proper notations and building blocks are required for modeling the photoemission cascades of hollow ions in terms of electron configurations, fine-structure multiplets (cascade blocks) and transition amplitudes as well as the well-known selection rules, which altogether give rise to the observed photon emission (d). These additional electrons also modify and broaden, for example, the $K\alpha$ ($2p_{1/2,3/2} - 1s$) inner-shell transitions owing to their coupling and interaction with the ionic core, and result overall in shifts of the observed photon spectra (e). Obviously, these cascades usually exhibit a (very) large complexity, and this remains true even, if only the dominant decay paths are taken into account [26,27].

2.3. Implementation of Atomic Cascades

To explore and analyze the photon emission from multiply charged and excited ions near surfaces, an easy-to-use but still powerful platform is needed in order to expand atomic theory towards the modeling of hollow-ion decay cascades [17]. JAC, the Jena Atomic Calculator [16,22], is such a platform that supports atomic (structure) calculations of different kind and complexity. Figure 2 displays selected applications of this toolbox for computing the interaction amplitudes, properties, as well as a good number of excitation and decay processes for open-shell atoms and ions. Based on Julia [28,29], a new programming language for scientific computing, this toolbox can be applied without much prior knowledge of either the language or the code. With the design and implementation of JAC, we aim to develop a descriptive language that (i) is simple enough for both novice and experienced users of this toolbox, (ii) emphasizes the underlying atomic physics, and (iii) avoids most technical slang common to many established electronic structure codes. All these goals are especially relevant for the simulation of atomic cascades and photon emission spectra, i.e., the focus of the present work [30,31].

Different atomic processes (and amplitudes) usually need to be combined for all cascades in order to model the behavior and observations of atoms and ions. To facilitate a systematic treatment of such cascades, JAC supports and distinguishes a number of *cascade schemes*, as briefly listed in the right panel of Figure 2. These schemes refer to different physical scenarios, such as the stepwise decay of inner-shell excited atoms via photon or

electron emission, their photoexcitation or ionization, the dielectronic capture of electrons by multiply and highly charged ions, or just the formation and decay of hollow ions.

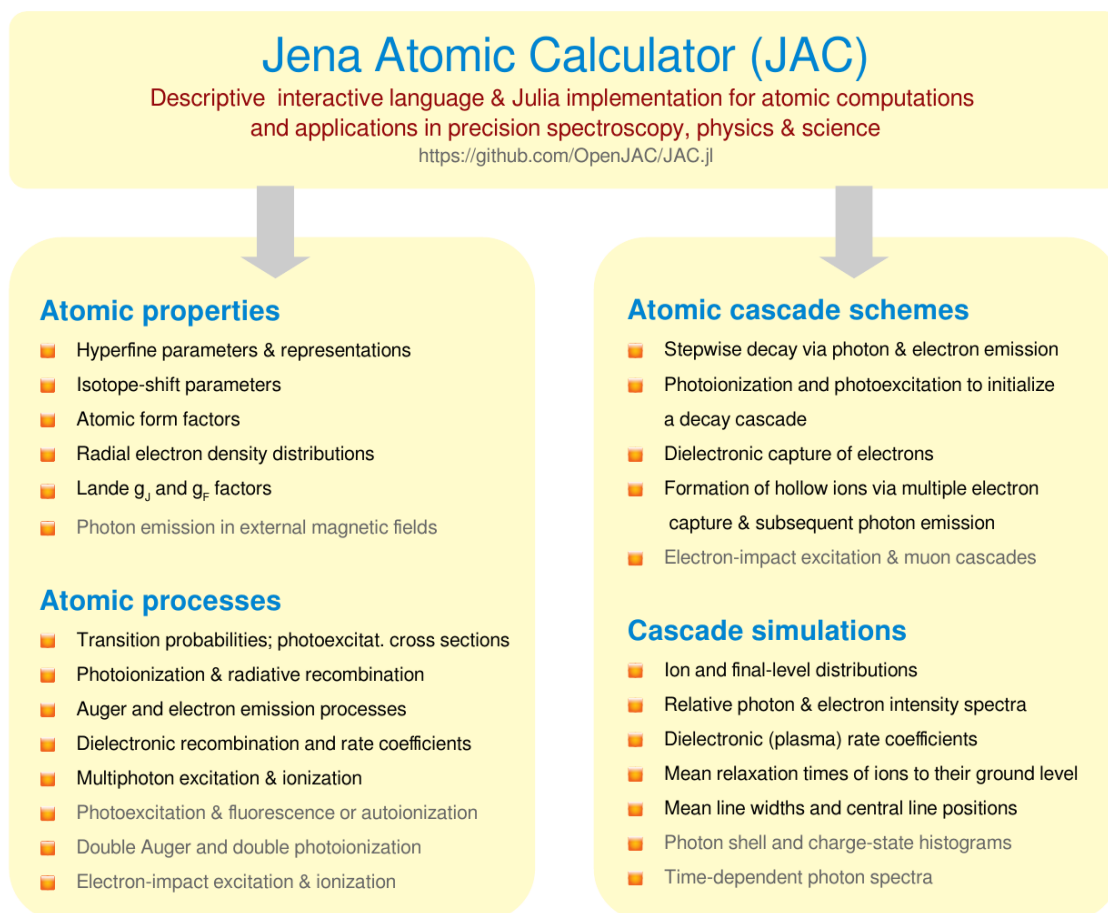


Figure 2. Selected applications of the JAC toolbox that help calculate atomic properties, processes and cascades. See Refs. [16,30] for a detailed account of the various features of this toolbox.

From a physics viewpoint, of course, rather different observations from atomic cascades, such as photon, electron or ion distributions, can normally be traced back to the same set of elementary processes and amplitudes and, hence, make recalculation of these amplitudes unnecessary, not to say cumbersome. To deal with the setup (and analysis) of different experiments, the JAC toolbox therefore clearly distinguishes between cascade *computations* and *simulations*. While a cascade computation aims to calculate and collect the (many-electron) amplitudes and rates for all relevant pathways of a cascade, the subsequent simulation then makes use of these precompiled data in order to derive the ion, photon or electron distributions, various rate coefficients or any other wanted information. These cascade simulations are typically much faster than the prior computations, and similar simulations are often performed repeatedly based on the same data. This work adds the decay of *hollow* ions as a new cascade scheme to JAC, owing to the placement of multiple electrons into (and their distribution among) different valence shells, and together with the subsequent photon emission from these ions. Like the other schemes that are available in JAC for *doing* cascade computations [17], the hollow-ion scheme is built upon a list of automatically generated electron configurations and all their associated fine-structure levels as they are temporally occupied during the stepwise photon emission.

2.4. Data Types for Modeling Photon Spectra

The complexity of the emission and autoionization pathways of hollow-ion cascades requires special care for its implementation. To facilitate communication *with* and data

transfer *within* the program, the JAC toolbox is built upon a good number of well-designed data structures in order to define useful and frequently recurring objects for the representation and treatment of atoms and ions. These data structures also form the (language) elements in order to describe and control the desired computations.

Two prominent examples of such data structures are an `Orbital` for specifying the quantum numbers and radial components of single-electron orbital functions, and a `Level` for the full representation of a single ASF: $|\alpha JM\rangle$, and which encompasses all information about the radial wave functions, the coupling of the angular momenta and the mixing (and number) of CSF within the given basis. In total, there are at present about ~ 250 of these data structures in JAC, though most of them remain hidden from the user. In this update to the code, the set of data structures has been enlarged by several types in order to explore, analyze and demonstrate the photon emission from hollow ions due to the placement of additional electrons into outer shells. Figure 3 displays the definition of the data structure `Cascade.HollowIonScheme` in JAC that helps perform all the cascade computations. In particular, it allows selection of one of the possible schemes of a `Cascade.Computation` and enables the user to specify the atomic processes that are to be included in the relaxation and multipole transitions for the coupling of the radiation field, as well as the number of additional electrons to be included into the computations. It also requests the user to provide a list of nonrelativistic subshells (`intoShells`) into which the electrons are placed initially, and a second list (`decayShells`) for designating possible decay paths in addition to those shells that already belong to the ionic core. The core occupation of all ions in terms of one or several reference configurations is common to all cascade schemes and provided independently of the cascade computations. A flexible but powerful description of this shell occupation as well as of further input is needed in order to cover the range of possible applications in atomic, plasma and surface physics, in which hollow ions frequently occur. Moreover, various methods exist and can be utilized interactively in JAC in order to readily generate and manipulate the different shell lists.

```

struct Cascade.HollowIonScheme <: Cascade.AbstractCascadeScheme
    ... a data type to specify and describe the decay of hollow ions due to the placement of several
    electrons into different (Rydberg) shells, with regard to an ionic core configuration, and to
    which one or several electrons are added into high nl shells. The shell lists for both, the
    initial placement of electrons (intoShells) and their subsequent decay (decayShells) need to
    be specified explicitly in order to readily control the size of the computations.

+ processes          ::Array{Basics.AbstractProcess,1}
    ... List of atomic processes that are supported and should be included into the decay scheme.
+ multipoles         ::Array{EmMultipole,1}
    ... Multipoles of the radiation field for the radiative stabilization processes.
+ NoCapturedElectrons ::Int64
    ... Number of captured electrons, e.g. placed in the intoShells.
+ intoShells         ::Array{Shell,1}
    ... List of (nonrelativistic) shells into which electrons are to be placed (captured) initially.
+ decayShells        ::Array{Shell,1}
    ... List of shells into which the excited electrons can decay (in addition to the core shells).

```

Figure 3. Definition of the data structure `Cascade.HollowIonScheme` in JAC that helps perform the cascade computations in Section 3 below. It selects one of the possible schemes of a `Cascade.Computation` and enables the user to specify the atomic processes and the multipole components of the radiation field that are to be included in the nonradiative and radiative stabilization of ions.

Apart from the hollow-ion cascade scheme above, Table 1 displays several other data structures that are relevant for the computation and analysis of photon emission (or electron) spectra. They are explained just briefly here, while further details can readily be obtained from the JAC toolbox manual [30] or by using Julia's help facilities [32]. Nonetheless, these

data structures are relevant for the reader (and users of JAC) to better understand and possibly control the spectra of hollow ions that need to be synthesized.

Table 1. Selected data structures of the JAC toolbox that are relevant for the calculation and analysis of photon emission spectra. Here, only a brief explanation is given, while further details can be found by using Julia’s help facilities.

Structures and Brief Explanation

`Cascade.AbstractCascadeApproach`: defines an abstract type for dealing with the cascade approach that is to be applied to the generation of all atomic levels and the evaluation of many-electron amplitudes.

`Cascade.AbstractCascadeScheme`: specifies an abstract data type to discriminate between different excitation, ionization and decay schemes of an atomic cascade; see Ref. [17] for a detailed discussion of different cascade schemes in JAC.

`Cascade.AbstractSimulationProperty`: defines an abstract type to deal with the property or distribution that is to be simulated, based on given cascade data; see below for several concrete types (properties).

`Cascade.Computation`: defines a data structure for the computation of a photoexcitation, photoionization, stepwise decay or hollow-ion cascade, and likely a few more in the future.

`Cascade.Simulation`: defines a structure to deal with cascade simulations of various kinds, based on given data from prior cascade computations.

`Cascade.IonDistribution`: defines a type to simulate the (final) ion or charge-state distribution, once all cascade computations are completed.

`Cascade.PhotonIntensity`: a type to simulate the photon intensities as applied and shown in Section 3; cf. also `Cascade.ElectronIntensity`.

`Cascade.MeanRelaxationTime`: a type to determine the mean relaxation times for given levels or configurations, i.e., the time, in which 70 %, 80 % or 90 % decay back to their ground configuration.

`Cascade.DrRateCoefficients`: a type to simulate the DR plasma rate coefficients as function of the plasma temperature.

3. Photon Satellite Emission from Hollow Ions

Near matter, multiply charged ions typically capture by charge transfer a good number of electrons, and this applies especially if metallic surfaces are approached. Apart from the rapid electron capture and re-emission (i.e., autoionization) processes, these ions also stabilize by photon emission and then give rise to arrays of unresolved lines. For an incident beam of Ar^{17+} ions, for example, Briand et al. [2] observed well-separated lines of comparable intensity owing to the occurrence of the KL^m ($2 \leq m \leq 8$) configurations with a single K-shell hole but multiple holes in the L shell, and likely further electrons in the M shells. For the sake of illustration, here we shall analyze the $\text{K}\alpha$ photon emission spectra from KL^mM^n configurations of Ar^{q+} ($q = 9 \dots 16$) ions for their shift and occurrence of additional lines in the spectra as well as for their mean relaxation time, although other spectra and tasks could be examined along quite similar lines.

3.1. $\text{K}\alpha^s$ Satellite Emission from KLM^n Configurations

Additional electrons (or holes) in valence shells generally shift and also alter the line shape of all core-shell transitions owing to their fine-structure and coupling to the core electrons. Both of these contributions increase with the number of electrons in outer shells but are expected to *decrease*, if the principal quantum number n of these shells becomes sufficiently large. Following the observations by Briand et al. [1], we wish here to simulate and compare the $\text{K}\alpha^s$ satellite emission spectra of initially KL_{23} , KL_{23}M and KL_{23}M^2 hollow-ion configurations, i.e., the region of the $2p \rightarrow 1s$ emission lines for Ar^{q+} ($q = 14 \dots 16$) ions. Emphasis is placed on how these $\text{K}\alpha^s$ lines depend on the number of valence-shell electrons, the treatment of the autoionization, and how readily these spectra can be synthesized by means of the JAC toolbox. In addition to the photon spectra, of course, the electron emission and fluorescence yields are affected by the population of the valence shells, which will not be considered here.

Let us first consider the $K\alpha^s$ photon spectra of Ar^{15+} ions with an initial KL_{23}M configuration, and which decays both by electron and photon emission. Figure 4 displays the (Julia) input for performing the requested cascade computations and simulations associated with the $K\alpha^s (2p \rightarrow 1s)$ emission. For a hollow-ion cascade, the initial-shell occupation has to be provided by the user, although different electron distributions of the valence shells can be chosen and are supported by the program. In the given example, a single electron in the $3s$, $3p$ or $3d$ shells (`intoShells`) is added to a $1s2p$ ionic core to form one of the KL_{23}M configurations. All these initial configurations can decay either radiatively or by electric-dipole (E1) transitions into any $1s + 2s + \dots + 3d$ orbitals (`decayShells`). Apart from the nuclear charge $Z = 18$ and the radial grid, moreover, the cascade *approach* for the generation of the ASF and the hollow-ion cascade scheme need to be specified in order to follow the relaxation of the ions down to the $1s^22s$ or $1s^2$ ground configurations. Once this input has been specified (and assigned to the variable `comp`), we just need to perform() the computation in order to automatically generate the lists of multiplets and transition data, and to write them to disk by a call to the JLD library. In the subsequent simulations, these data are *read in* to generate different spectra and distributions. In the lower panel of Figure 4, we derive the photon intensities of the Ar^{15+} ions above in the energy interval 113 ... 116 Hartree $\approx 3075 \dots 3150$ eV that comprises the $K\alpha_{12}$ lines of helium-like argon [33], and where we assumed an equal distribution of the captured electron among the $3s + 3p + 3d$ shells (`leadingConfigs`). While we shall not explain here all the details in Figure 4, overall it shows how readily cascade computations and simulations can be performed and controlled in order to model different decay cascades. Note that all assignments from the input of Figure 4 can be also called and tested interactively, and that very similar input to JAC has been applied for generating all other spectra and figures in this section.

```
# Hollow-ion cascade computations for an  $\text{KL}_{23}\text{M}^m$  ( $m=0, 1, 2$ ) configurations, cf. Figure 5
setDefault("unit: energy", "eV")
grid      = Radial.Grid(Radial.Grid(false), rnt = 4.0e-6, h = 5.0e-2, hp = 0.6e-2, rbox = 10.0)
name      = "Hollow-ion cascade for  $\text{KL}_{23}\text{M}^n$  configurations"
intoShells = Basics.generateShellList(3, 3, "d")
decayShells = Basics.generateShellList(1, 3, "d")
ionScheme  = Cascade.HollowIonScheme([Radiative(), Auger()], [E1], 1, intoShells, decayShells)

comp      = Cascade.Computation(Cascade.Computation(); name=name, nuclearModel=Nuclear.Model(18.),
                                grid=grid, approach=Cascade.SCA(), scheme=ionScheme,
                                initialConfigs=[Configuration("1s 2p")] )
perform(comp)

# Simulation of the photon emission from the hollow-ion cascade, cf. Figure 5
simulationSettings = Cascade.SimulationSettings(true, false, 0.)
name              = "Photon emission simulations for the ions from above"
data              = [JLD.load("cascade-hollow-ion-computations.jld")]
leadingConfigs    = [Configuration("1s 2p 3s"), Configuration("1s 2p 3p"), Configuration("1s 2p 3d")]
prop              = Cascade.PhotonIntensities(113., 116., Tuple{Int64,Float64}[], leadingConfigs)

simu             = Cascade.Simulation(Cascade.Simulation(), name=name, settings=simulationSettings,
                                       computationData=data, property=prop )
perform(simu)
```

Figure 4. Julia input for generating the green spectrum in Figure 5 for an initial KL_{23}M configuration of Ar^{15+} ions; this input describes the cascade computation (upper panel) as well as the associated cascade simulation (lower panel). See text for further explanations. This figure also demonstrates how readily JAC can be employed in order to generate various spectra and properties. However, no attempt is made to explain this input in full detail, for which we refer the reader to either the manual [30] of the JAC toolbox or the REPL [32].

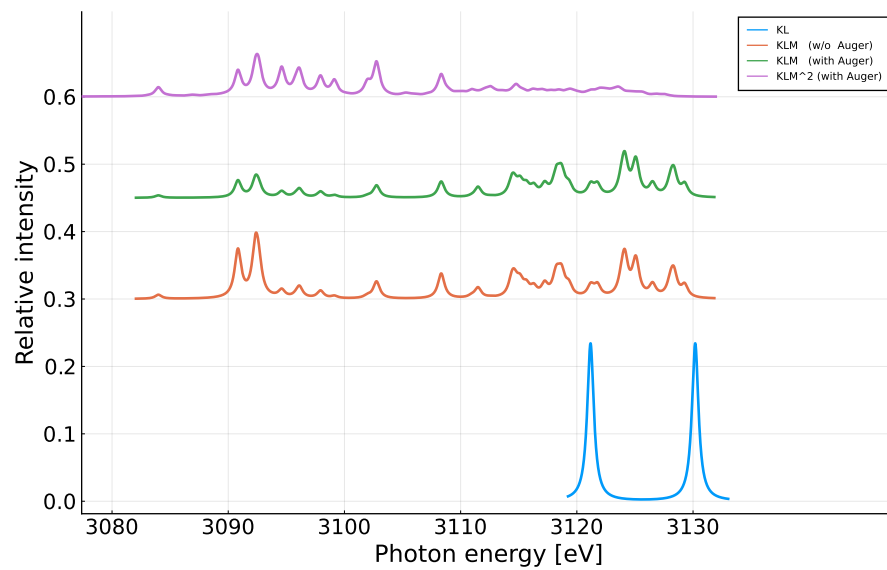


Figure 5. Comparison of the (relative) photon intensity distribution near the $K\alpha^s$ ($2p - 1s$) resonance lines of Ar^{q+} ($q = 14 \dots 16$) ions in KLM^n configurations. Simulated photon spectra are shown for an initial KL_{23} configuration (blue spectrum), KL_{23}M without autoionization (orange spectrum), KL_{23}M with autoionization (green spectrum) and the KL_{23}M^2 configurations (violet spectrum). To separate these spectra, they are shifted relative to each other by a constant background, and a line width $\Gamma = 1$ eV is assumed in all cases. See text for further explanations.

Figure 5 displays and compares the (relative) photon intensity distribution near the two $K\alpha_{12}$ ($2p_{1/2,3/2} - 1s$) resonance lines of Ar^{q+} ($q = 14 \dots 16$) ions in initially the KL_{23} (blue spectrum), KL_{23}M (orange and green spectra) as well as the KL_{23}M^2 configurations (violet spectrum), if a $2p$ electron is assumed in the L_{23} shell, and if the M-shell electrons are equally placed into the $3s + 3p + 3d$ shells. For the KL_{23}M configuration, moreover, we display the emission spectrum without the competitive Auger processes (orange spectrum) and by taking all autoionization channels into account (green spectrum). Quite sizable differences occur even in the region of the well-studied $K\alpha_{12}$ emission if additional electrons occupy outer shells, owing to the extended fine-structure and Auger processes that contribute to the cascades. While a single electron in one of the $3s + 3p + 3d$ shells just leads to a fine-structure of about 45 eV, the high-energy peaks are clearly lowered if a second electron appears in the M shells. Here, a constant width of ~ 1 eV is assumed in all four photon spectra in order to account for some characteristic experimental resolution. Although the natural widths of these lines could also be computed by means of the JAC toolbox, the observed X-ray spectra are often determined by the resolution $\Delta E/E \lesssim 0.005$ of typical detectors in the mid X-ray region. For the sake of simplicity, moreover, all cascade computations have been performed in E1 approximation and by considering all decay configurations independent of each other. The computational effort rapidly increases with the number of M-shell electrons and for the KL_{23}M^2 (violet) spectrum already includes more than 20,000 fine-structure transitions.

As typical for JAC, all the underlying transition amplitudes in Figure 5 have been calculated ab initio without any scaling of radial integrals and/or matrix elements. Formally, one can shift all the photon (electron) energies by a constant amount in order to account for those contributions that cannot be included so easily in the cascade computations, such as QED shifts or the coupling of levels to the continuum. Moreover, since the cascade computations are typically based on the independent decay of single configurations, the accuracy of the photon lines in Figure 5 is mainly restricted by missing correlations and is estimated to be $\lesssim 5$ eV. This accuracy might be improved by going beyond the single-configuration approach (cf. `Cascade.SCA()` in Figure 4), but this then results in much larger computations, which have not been considered so far.

Figure 5 already elucidates the complexity in describing and analyzing hollow-ion cascades as one first needs to place the valence electron(s) into some proper shells in order to form all relevant KLM^n fine-structure levels, and second, one needs to follow their subsequent—radiative and/or nonradiative—decay pathways. It is *this* interplay of radiative and nonradiative processes that generally gives rise to the rich $K\alpha^s$ ($2p \rightarrow 1s$) emission, and with several further lines, especially at higher photon energies (not shown in this figure) if additional electrons occur in M and/or higher shells. The integral over these spectra is hereby equal to the mean number of photons that are emitted during the stabilization and, hence, just 1/2 for the helium-like KL configuration alone if all four $1s2p\ ^1P$ and $\ ^3P$ levels are populated equally. Here, the photon number 1/2 occurs since the two $\ ^3P_{0,2}$ levels cannot decay by (single-photon) E1 emission to the $1s^2\ ^1S_0$ within the given cascade scheme. For KLM^n configurations, furthermore, the mean photon number is typically <1 because of the autoionization, but increases again with the nuclear charge and the number of radiative transitions that contribute (at quite different frequencies) to the overall stabilization. The (relative) intensity of these spectra therefore also displays the efficiency with which these lines can be observed experimentally.

3.2. Mean Relaxation Time of KL^m Configurations

Ions with multiple inner-shell holes decay stepwise along many different pathways, i.e., sequences of fine-structure levels that are connected by different electron and photon emission processes. These pathways are associated with quite different relaxation times, which the ions take to relax to their ground configuration. While the decay of individual ionic levels occurs statistically according to their branching fractions and lifetimes, not much is known so far about the mean relaxation time that is needed in order to bring a sizable fraction of inner-shell excited ions back to their ground level (or configuration). Here, we define the *mean* relaxation time t_r such that, say, 70%, 80% or 90% of the ions are found in their ground configuration, if the electron(s) had been initially placed into any excited configuration such as KL^mM^n , or similar.

Figure 6 shows the mean relaxation time of Ar^{q+} ($q = 9 \dots 16$) ions in initial KL^m configurations for returning back to their associated ground configurations. Here, the electrons in the L shells are distributed statistically among the 2s and 2p subshells. Both the radiative decay and autoionization of the ions are taken into account and give rise to ions in charge states with either $Z - q$ or $Z - q - 1$ electrons. The times for the relaxation of 70% (blue line), 80% (orange line) and 90% (green line) are compared and typically follow a similar trend. These relaxation times are essentially determined by the lowest decay rates and the number of ions that follow the different pathways. For ions in the initial KL ($m = 1$) configuration, the $1s2s\ ^1S_0$ and $1s2p\ ^3P_{0,2}$ levels cannot decay by single-photon transitions, but will relax by collisional de-excitation or two-photon transitions down to the $1s^2\ ^1S_0$. For equally distributed L-shell electrons and the two given decay mechanisms (E1 + Auger), therefore, only 84% can reach the ground configuration. Similar reasons also apply to the rather long relaxation times for the KL^3 configurations, for which the slow $2p - 2s$ transitions eventually determine the relaxation to the ground configuration. While Figure 6 just displays an ad hoc example for the mean relaxation time of hollow ions, a similar analysis for other (hollow) ions may help understand and model the population dynamics of ions under various (plasma) conditions.

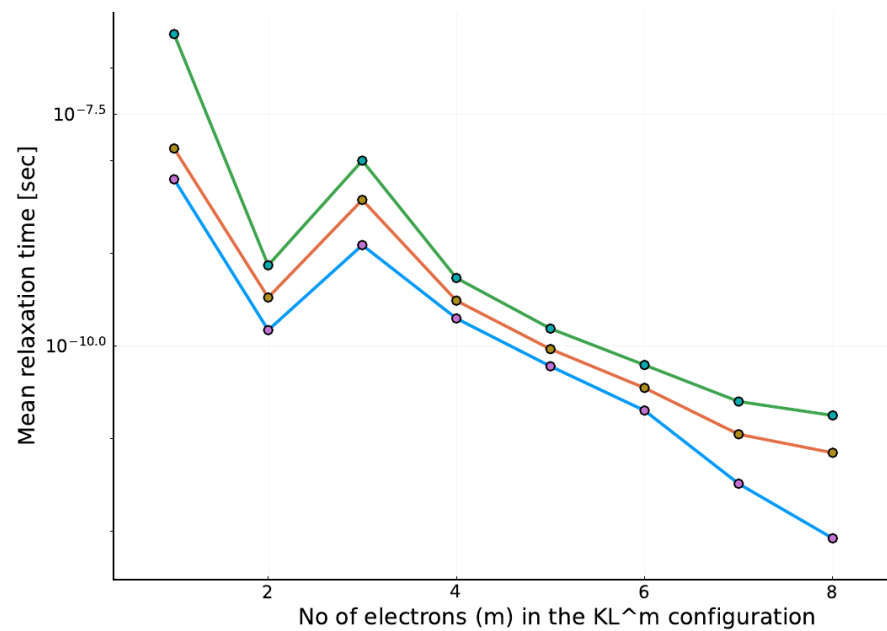


Figure 6. Mean relaxation time of Ar^{q+} ($q = 9 \dots 16$) ions in initial KL^m configurations for returning back to their $Z - q$ and $Z - q - 1$ electron ground configurations with a $1s^2$ filled K shell. The L-shell electrons are assumed to be distributed statistically among the $2s$ and $2p$ subshells, and both the radiative decay and autoionization of the ions are taken into account. The mean relaxation times are compared for the stabilization of 70% (blue line), 80% (orange line) and 90% (green line). Here, the thin colored lines are just shown to guide the eyes.

3.3. Analysis of Further Photon and Electron Spectra

The inherent complexity of atomic cascades becomes visible at various places, including absorption studies and applications of different kinds in astro-, plasma and surface physics. In the inner-shell photoexcitation and ionization of atoms or (negative) ions, a detailed modeling of these cascades has helped explore the ion distribution as function of the photon energy [34,35] and has revealed differences in the observed photon spectra from different astrophysical sources [36,37]. In plasma physics, moreover, the spectra of hollow ions are frequently analyzed for diagnostic purposes.

Apart from these applications, the simulation of hollow-ion cascades opens the route to investigations that have thus far been neglected in the literature due to their complexity. A few interesting research questions refer to:

- How can the effective electron capture be characterized for ions that swiftly collide with surfaces or rest-gas atoms? How can one model the relaxation dynamic of such ions that have been found to be inconsistent with prior measurements [12]?
- Which additional X-ray lines occur, and with which intensity, if electrons are placed into high- n Rydberg shells? Which of these lines contribute due to non-E1 (dipole) transitions? Such studies may have impacts on different kinds of precision measurements.
- How do the radiative (multipole) and Auger transition rates interplay with each other for muonic X-ray spectra following the capture of a muon by an atom?
- In two-step Auger cascades, a coherent summation over the individual decay paths from the first and second steps is known to be necessary in order to predict the angular distribution of the emitted Auger electrons if the fine-structure splitting of two or more intermediate levels is small or comparable to the natural line widths of these levels [38,39]. How can such a *coherence transfer* be treated efficiently, if needed, for a whole cascade?
- How do radiative and dielectronic capture compete with each other under different experimental conditions?

- A good understanding of astrophysical light curves helps resolve the chemical evolution of the early universe and, eventually, the formation and growth of galaxies. However, very little is known so far about the optical properties of the heavy r-process elements, and, hence, most previous light-curve models still utilize the opacities from the iron-group elements. How does a proper treatment of the opacities and atomic cascades affect the light curve as observed, for instance, from neutron-star mergers?

These and several related questions can be addressed more or less readily by means of the JAC toolbox and, especially, by applying the present extension for modeling hollow-ion cascades.

4. Summary and Conclusions

Obviously, a rather large number of relaxation processes typically emerge when multiply charged ions approach surfaces. Apart from the rapid capture and re-emission of electrons by the ions, the photon spectra may provide unique fingerprints on their relaxation and neutralization. A detailed modeling of the associated cascades, including more-or-less accurate predictions of cross sections and rates, is needed for understanding the photon emission and, hence, the first steps of the relaxation.

In this work, we have shown and discussed how additional electrons in outer (valence) shells shift and modify the observed photon spectra. Examples refer to the KL^mM^n configurations of Ar^{q+} ions as they have been observed in swift ion-surface collisions. All simulations were performed using the JAC toolbox [16], which integrates different atomic processes within a single computational framework and has now been expanded to facilitate the computation and simulation of photon emission cascades from hollow ions. These extensions make JAC an excellent tool to model cascades of further kind and complexity in the future.

Funding: This research received no external funding.

Conflicts of Interest: The author declares no conflict of interest.

References

1. Briand, J.-P.; de Billy, L.; Charles, P.; Essabaa, S.; Briand, P.; Geller, R.; Desclaux, P.; Bliman, S.; Ristori, C. Production of hollow atoms by the excitation of highly charged ions in interaction with a metallic surface. *Phys. Rev. Lett.* **1990**, *65*, 159. [[CrossRef](#)] [[PubMed](#)]
2. Briand, J.-P.; Giardino, G.; Borsoni, G.; Froment, M.; Eddrief, M.; Sebenne, C.; Bardin, S.; Schneider, D.; Jin, J.; Khemliche, H.; et al. Decay of hollow atoms above and below a surface. *Phys. Rev. A* **1996**, *54*, 4136. [[CrossRef](#)] [[PubMed](#)]
3. Palmeri, P.; Quinet, P.; Zitane, N.; Vaeck, N. Calculation of Auger rates for complex hollow-atom configurations. *J. Phys. B* **2001**, *34*, 4125. [[CrossRef](#)]
4. Vaeck, N.; Hansen, J.E.; Palmeri, P.; Quinet, P.; Zitane, N.; Godefroid, M.; Fritzsche, S.; Kylstra, N. Hollow atoms: A theoretical challenge. *Phys. Scr.* **2001**, *T95*, 68. [[CrossRef](#)]
5. Tokesi, K.; Wirtz, L.; Lemell, C.; Burgdörfer, J. Hollow-ion formation in microcapillaries. *Phys. Rev. A* **2001**, *64*, 042902. [[CrossRef](#)]
6. DuBois, R.D.; Tokesi, K.; Giglio, E. Charge deposition, redistribution, and decay properties of insulating surfaces obtained from guiding of low-energy ions through capillaries. *Phys. Rev. A* **2019**, *99*, 062704. [[CrossRef](#)]
7. Schippers, S.; Martins, M.; Beerwerth, R.; Bari, S.; Holste, K.; Schubert, K.; Viefhaus, J.; Savin D.W.; Fritzsche, S.; Müller, A.; et al. Near L-edge single and multiple photoionization of singly charged iron ions. *Astrophys. J.* **2017**, *849*, 5. [[CrossRef](#)]
8. Beerwerth, R.; Buhr, T.; Perry-Sassmannshausen, A.; Stock, S.O.; Bari, S.; Holste, K.; Kilcoyne, A.L.D.; Reinwardt, S.; Ricz, S.; Savin, D.W.; et al. Near L-edge single and multiple photoionization of triply charged iron ions. *Astrophys. J.* **2019**, *887*, 189. [[CrossRef](#)]
9. Hansen, S.B.; Colgan, J.; Faenov, A.Y.; Abdallah, J., Jr.; Pikuz, S.A.; Skobelev, I.Y.; Wagenaars, E.; Booth, N.; Culfa, O.; Dance, R.J.; et al. Detailed analysis of hollow ions spectra from dense matter pumped by X-ray emission of relativistic laser plasma. *Phys. Plasma* **2014**, *887*, 189. [[CrossRef](#)]
10. Gillaspay, J.D. Precision spectroscopy of trapped highly charged heavy elements: Pushing the limits of theory and experiment. *Phys. Scr.* **2014**, *89*, 1114004. [[CrossRef](#)]
11. Chantler, C.T.; Payne, A.T.; Gillaspay, J.D.; Hudson, L.T.; Smale, L.F.; Henins, A.; Kimpton, J.A.; Takacs, E. X-ray measurements in helium-like atoms increased discrepancy between experiment and theoretical QED. *New J. Phys.* **2014**, *16*, 123037. [[CrossRef](#)]
12. Wilhelm, R.A.; Gruber, E.; Schweska, J.; Kozubek, R.; Madeira, T.I.; Marques, J.P.; Kobus, J.; Krasheninnikov, A.V.; Schleberger, M.; Aumayr, F. Interatomic Coulombic decay: The mechanism for rapid deexcitation of hollow atoms. *Phys. Rev. Lett.* **2017**, *119*, 103401. [[CrossRef](#)] [[PubMed](#)]

13. Sisourat, N.; Engin, S.; Gorfinkiel, J.; Kazandjian, S.; Kolorenc, P.; Miteva, T. On the computations of interatomic Coulombic decay widths with R-matrix method. *J. Chem. Phys.* **2017**, *146*, 244109. [[CrossRef](#)] [[PubMed](#)]
14. Khokhlova, M.; Bahmanpour, L.; Bachhawat, N.; Cooper, B.; Averbukh, V. Interatomic Coulombic decay rate in endohedral complexes. *J. Phys.* **2020**, *B53*, 184002. [[CrossRef](#)]
15. Jakas, M.M.; Harrison, D.E., Jr. Many-body effects in atomic-collision cascades. *Phys. Rev. Lett.* **1985**, *5*, 1782. [[CrossRef](#)]
16. Fritzsche, S. A fresh computational approach to atomic structures, processes and cascades. *Comp. Phys. Commun.* **2019**, *240*, 1. [[CrossRef](#)]
17. Fritzsche, S.; Palmeri, P.; Schippers, S. Atomic cascade computations. *Symmetry* **2021**, *13*, 520. [[CrossRef](#)]
18. Cowan, R.D. *The Theory of Atomic Structure and Spectra*; University of California Press: Berkeley, CA, USA, 1981.
19. Johnson, W.R. *Atomic Structure Theory: Lectures on Atomic Physics*; Springer: Berlin/Heidelberg, Germany, 2007.
20. Fritzsche, S. Large-scale accurate structure calculations for open-shell atoms and ions. *Phys. Scr.* **2002**, *T100*, 37. [[CrossRef](#)]
21. Grant, I.P. *Relativistic Quantum Theory of Atoms and Molecules: Theory and Computation*; Springer: Berlin/Heidelberg, Germany, 2007.
22. Fritzsche, S. The RATIP program for relativistic calculations of atomic transition, ionization and recombination properties. *Comp. Phys. Commun.* **2012**, *183*–1525. [[CrossRef](#)]
23. Perry-Sassmannshausen, A.; Buhr, T.; Borovik, A., Jr.; Martins, M.; Reinwardt, S.; Ricz, S.; Stock, S.O.; Trinter, F.; Muller, A.; Fritzsche, S.; et al. Multiple photodetachment of carbon anions via single and double core-hole creation. *Phys. Rev. Lett.* **2020**, *124*, 083203. [[CrossRef](#)]
24. Sobel'man, I.L.; Vainshtein, L.; Yukov, E.A. *Excitation of Atoms and Broadening of Spectral Lines*; Springer: Berlin/Heidelberg, Germany, 1995.
25. Allen, F.I.; Biedermann, C.; Radtke, R.; Fussmann, G.; Fritzsche, S. Energy dependence of angular momentum capture states in charge exchange collisions between slow highly charged argon ions and argon neutrals. *Phys. Rev. A* **2008**, *78*, 032705. [[CrossRef](#)]
26. Schippers, S.; Beerwerth, R.; Abrok, L.; Bari, S.; Buhr, T.; Martins, M.; Ricz, S.; Viefhaus, J.; Fritzsche, S.; Muller, A. Prominent role of multielectron processes in K-shell double and triple photodetachment of oxygen anions. *Phys. Rev. A* **2016**, *94*, 041401(R). [[CrossRef](#)]
27. Schippers, S.; Buhr, T.; Borovik, A., Jr.; Holste, K.; Perry-Sassmannshausen, A.; Mertens, K.; Reinwardt, S.; Martins, M.; Klumpp, S.; Schubert, K.; et al. The photon-ion merged-beams experiment PIPE at PETRA III—The first five years. *X-ray Spec.* **2020**, *49*, 11. [[CrossRef](#)]
28. Available online: <https://docs.julialang.org/> (accessed on 10 February 2022).
29. Bezanson, J.; Chen, J.; Chung, B.; Karpinski, S.; Shah, V.B.; Vitek, J.; Zoubritzky, J. Julia: Dynamism and performance reconciled by design. *Proc. ACM Program. Lang.* **2018**, *2*, 120. [[CrossRef](#)]
30. Fritzsche S. JAC: User Guide, Compendium & Theoretical Background. Available online: <https://github.com/OpenJAC/JAC.jl> (accessed on 10 February 2022).
31. Fritzsche, S.; Fricke, B.; Sepp W.D. Reduced L_1 level-width and Coster-Kronig yields by relaxation and continuum interactions in atomic zinc. *Phys. Rev. A* **1992**, *45*, 1465. [[CrossRef](#)]
32. Julia Comes with a Full-Featured Interactive and Command-Line REPL (Read-Eval-Print Loop) That Is Built into the Executable of the Language. Available online: <https://julialang.org/> (accessed on 10 February 2022).
33. Kramida, A.; Ralchenko, Y.; Reader, J.; NIST ASD Team. NIST Atomic Spectra Database (ver. 5.8). 2021. Available online: <https://physics.nist.gov/asd> (accessed on 25 February 2022).
34. Schippers, S.; Beerwerth, R.; Bari, S.; Buhr, T.; Holste, K.; Kilcoyne, A.L.D.; Perry-Sassmannshausen, A.; Phaneuf, R.A.; Reinwardt, S.; Savin, W.; et al. Near L-edge single and multiple photoionization of doubly charged iron ions. *Astrophys. J.* **2021**, *908*, 52. [[CrossRef](#)]
35. Müller, A.; Martins, M.; Borovik, A., Jr.; Buhr, T.; Perry-Sassmannshausen, A.; Reinwardt, S.; Ricz, S.; Trinter, F.; Schippers, S.; Fritzsche, S.; et al. The role of L-shell single and double core-hole production and decay in m -fold ($m = 1, 2, \dots, 6$) photoionization of the Ar^+ ion. *Phys. Rev. A* **2021**, *104*, 033105. [[CrossRef](#)]
36. Lee, J.C.; Iwasawa, K.; Houck, J.C.; Fabian, A.C.; Marshall, H.L.; Canizares, C.R. The shape of the relativistic iron $K\alpha$ line from MCG-6-30-15 measured with the Chandra HETGS and RXTE. *Astrophys. J.* **2002**, *570*, 147. [[CrossRef](#)]
37. Hanke, M.; Wilms, J.; Nowak, M.A.; Pottschmidt, K.; Schulz, N.S.; Lee, J.C. Chandra X-ray spectroscopy of the focused wind in the Cygnus X-1 system I. The non-dip spectrum in the low/hard state. *Astrophys. J.* **2009**, *690*, 330. [[CrossRef](#)]
38. Shimizu, Y.; Yoshida, H.; Okada, K.; Muramatsu, Y.; Saito, N.; Okashi, H.; Tamenori, Y.; Fritzsche, S.; Kabachnik, N.M.; Tanaka, H.; et al. Ultra-high resolution angle-resolved measurement of Auger emission from the photoexcited $1s^{-1} \rightarrow 3p$ state of Ne. *J. Phys.* **2000**, *B33*, L685.
39. Ueda, K.; Shimizu, Y.; Chiba, H.; Kitajima, M.; Tanaka, H.; Fritzsche, S.; Kabachnik, N.M. Experimental and theoretical study of the Auger cascade following the $2p \rightarrow 4s$ photoexcitation in Ar. *J. Phys.* **2001**, *B34*, 107. [[CrossRef](#)]